Surfactant adsorption kinetics in microfluidics

Birte Riechers[a,b], Florine Maes[a,b], Elias Akoury[c,d,e], Benoît Semin[b,f,g,h,i], Philipp Gruner[b], and Jean-Christophe Baret[a,b,1]

[a]Soft Microsystems, Centre de Recherche Paul Pascal, Unité Propre de Recherche 8641, CNRS, University of Bordeaux, 33600 Pessac, France; [b]Droplets, Membranes and Interfaces, Max Planck Institute for Dynamics and Self-Organization, 37077 Goettingen, Germany; [c]Department of Biochemistry, Ludwig Maximilians University, 81377 Munich, Germany; [d]Gene Center, Ludwig Maximilians University, 81377 Munich, Germany; [e]Department for NMR-based Structural Biology, Max Planck Institute for Biophysical Chemistry, 37077 Goettingen, Germany; [f]Laboratoire de Physique Statistique, École Normale Supérieure, Université de Recherche Paris Sciences et Lettres, 75005 Paris, France; [g]Laboratoire de Physique Statistique, Université Paris Diderot Sorbonne Paris-Cité, 75005 Paris, France; [h]Laboratoire de Physique Statistique, Sorbonne Universités, Pierre and Marie Curie University, University of Paris 06, 75005 Paris, France; and [i]Laboratoire de Physique Statistique, CNRS, 75005 Paris, France

Edited by David A. Weitz, Harvard University, Cambridge, MA, and approved August 16, 2016 (received for review March 15, 2016)

Emulsions are metastable dispersions. Their lifetimes are directly related to the dynamics of surfactants. We design a microfluidic method to measure the kinetics of adsorption of surfactants to the droplet interface, a key process involved in foaming, emulsification, and droplet coarsening. The method is based on the pH decay in the droplet as a direct measurement of the adsorption of a carboxylic acid surfactant to the interface. From the kinetic measurement of the bulk equilibration of the pH, we fully determine the adsorption process of the surfactant. The small droplet size and the convection during the droplet flow ensure that the transport of surfactant through the bulk is not limiting the kinetics of adsorption. To validate our measurements, we show that the adsorption process determines the timescale required to stabilize droplets against coalescence, and we show that the interface should be covered at more than 90% to prevent coalescence. We therefore quantitatively link the process of adsorption/desorption, the stabilization of emulsions, and the kinetics of solute partitioning—here through ion exchange—unraveling the timescales governing these processes. Our method can be further generalized to other surfactants, including nonionic surfactants, by making use of fluorophore–surfactant interactions.

droplet | interfaces | surfactant | emulsion | microfluidics

Surface active compounds are ubiquitous in our daily life, be it in living systems or in industrial and technological products (1–3). The compounds are used widely for the stabilization of foams and emulsions for food and cosmetic products, painting materials, and industrial coatings (3). Emulsions are nowadays also used in combination with microfluidic systems for applications in biotechnology (3–11). An emulsion is a dispersion of one liquid phase into another, stabilized by surfactants in a metastable state. The kinetic stabilization of emulsions occurs through several mechanisms, involving electrostatic or steric repulsion and the buildup of Marangoni stresses to improve the lifetime of emulsions against coalescence (12, 13). On the other hand, surfactants are involved in transport processes such as Ostwald ripening or solute transport, which mediates the chemical equilibration of the system (14–17): in general, all processes affecting the lifetime of emulsions (coalescence, rupture, exchange, and loss of molecules) are directly related to the physics and dynamics of the surfactant molecules at interfaces (3, 4, 6, 10, 11, 15, 16). The first analysis of surfactant layers dates back to the 18th century with Franklin's experiments (1) and the first comprehensive studies on adsorption kinetics by Ward and Tordai (18) and Langmuir (19). From this point, a wide variety of models describe the adsorption dynamics, accounting for all kinds of molecular effects at interfaces (20–26). We expect two limiting cases: (*i*) the adsorption is limited by the bulk transport toward the interface, leading to a local equilibrium between the surfactant interfacial concentration and the bulk concentration in the vicinity of the interface at all times; and (*ii*) the adsorption is limited by the adsorption/desorption rate constants at the interface, and the bulk concentration is homogeneous at all time. If the bulk transport is a diffusive process, and if the adsorption is given by a Langmuir model, diffusion is always negligible below a critical radius $R^\star = D/(k_{ads}\Gamma_\infty)$, where D is the diffusion coefficient, k_{ads} the adsorption rate, and Γ_∞ the maximal interfacial coverage (*SI Text* and Fig. S1). This cutoff radius $R^\star$ was initially proposed by Jin et al. and is of the order of 50 μm for a series of classic surfactants (27). As a consequence, understanding the kinetics of surfactant in emulsification conditions is not possible using large-volume methods such as—among others—Wilhelmy tensiometry or even pendant droplet tensiometry. These methods are likely transport-limited unless adsorption barriers emerge. To make the adsorption the limiting process, the droplet size should thus be small. Even if the adsorption is not modeled by a Langmuir isotherm, the conclusion remains qualitatively valid. In the presence of convection, the timescale of transport is controlled by the Sherwood Sh number, which compares the mass transfer with convection to the one in the purely diffusive regime (28). Thus, the effect of convection increases the cutoff radius by the Sherwood number Sh, leading to a new cutoff radius $R'^\star = Sh \times R^\star$. Molecular transport becomes negligible compared with adsorption kinetics for droplets even at larger dimensions. Such experiments using small sizes and convection have been performed by Alvarez et al. (25), showing the importance of reaching the kinetic regime to reliably extract adsorption constants. In our experiments, we consider here droplets moving in a microfluidic channel to increase the bulk transport by convection; we use droplet-based microfluidics to analyze the adsorption kinetics of a surfactant, overcoming the transport limitation. We use a perfluoropolyether (PFPE) with a

Significance

Surfactant adsorption to interfaces is a dynamic process of relevance for foaming, emulsification, and detergency. Although the process has been described for centuries now, the rational measurement of adsorption and desorption constants, as well as the modeling of the binding mechanism, is still subject to many assumptions. The prevalence of transport through the bulk in classic measurements limits the reliability of the analysis. Microfluidics provides a means to achieve small sizes and significant droplet velocity to alleviate the limiting step of surfactant bulk transport. Adsorption kinetics are measured directly to make a link among droplet stabilization, ion exchange, and coalescence.

Author contributions: J.-C.B. designed research; B.R. and J.-C.B. performed research; F.M., E.A., B.S., and P.G. contributed new reagents/analytic tools; B.R., B.S., and J.-C.B. analyzed data; and B.R., B.S., and J.-C.B. wrote the paper.

The authors declare no conflict of interest.

This article is a PNAS Direct Submission.

Freely available online through the PNAS open access option.

[1]To whom correspondence should be addressed. Email: jean-christophe.baret@u-bordeaux.fr.

This article contains supporting information online at www.pnas.org/lookup/suppl/doi:10.1073/pnas.1604307113/-/DCSupplemental.

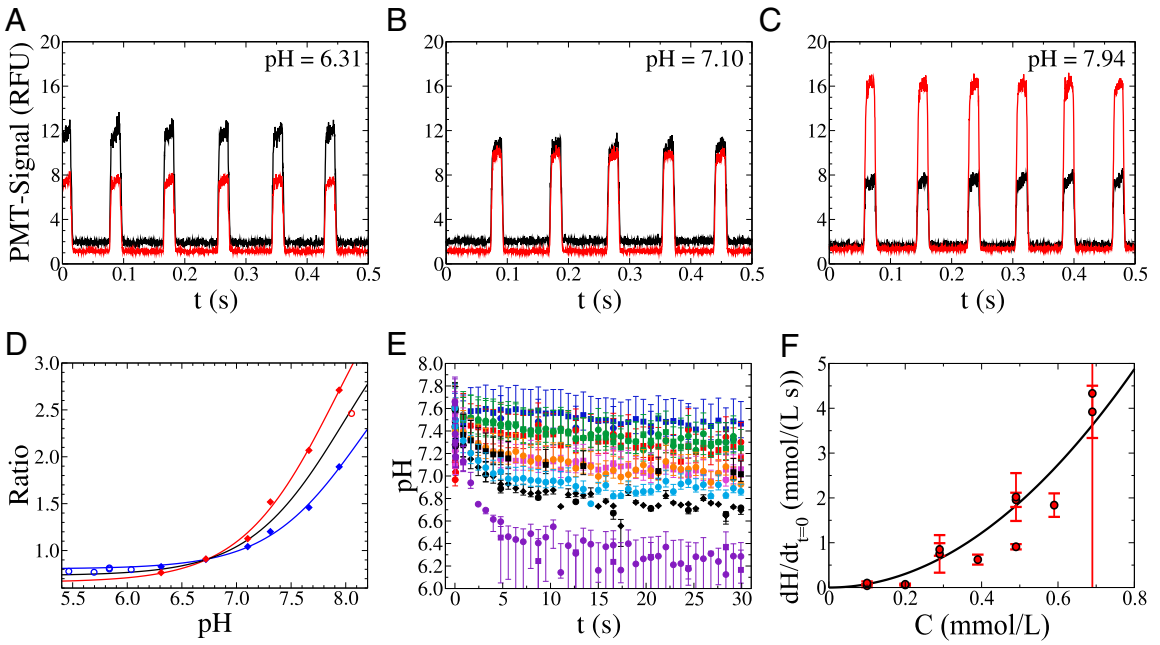

Fig. 1. (*A–C*) Signal of the different photomultipliers at higher (647 nm, red line) and lower (580 nm, black line) wavelength for a pH of the aqueous phase of 6.31 (*A*), 7.10 (*B*), and 7.94 (*C*). (*D*) Calibration of the ratio of the fluorescent signals in relation to the pH of the original solution [repetitions (red and blue) and mean (black)]. (*E*) pH change with time for surfactant concentrations of 0.05 mM (blue), 0.10 mM (red), 0.20 mM (green), 0.29 mM (pink), 0.39 mM (orange), 0.49 mM (black), 0.59 mM (light blue), and 0.69 mM (purple). The error bars show the uncertainty due to the calibration of the ratio of the signals versus the pH. (*F*) Speed of the reaction at time 0 for the different concentrations of surfactant used. The error bars correspond to the uncertainty on the fitting parameter (*SI Text* and Fig. S8).

carboxylic acid head group, soluble in the oil phase, as a model surfactant. We monitor the change of pH in the aqueous droplets produced on-chip as the surfactant adsorbs to the interface and releases its proton into the dispersed phase. From these experiments, we obtain a kinetic adsorption model, in a pure kinetic-limited adsorption regime. Another advantage of this technique is that the timescale of pH variation, which is used to obtain the adsorption rates, is much larger than the inverse of these adsorption rates. Equilibrium data are obtained independently and provide experimental values for the parameters required by the model. We finally address the issue of emulsion stability against coalescence (29): we compare the timescale of surfactant adsorption and the time above which droplets do not coalesce.

Experimental Results

We produce water-in-oil emulsions in microfluidics by dispersing a PBS solution into a continuous fluorous phase. A pH-sensitive fluorophore is used to measure the pH inside the droplets at different positions (and therefore time) inside the microfluidic channel using a fluorescence setup (*SI Text* and Fig. S2). The ratio of fluorescence intensities increases with increasing pH (Fig. 1 *A–C* *SI Text* and Fig. S3), and the pH measurement is sensitive and reliable in the range between 6.2 and 7.8 (Fig. 1*D*) (30). We determine the change in pH with time (corresponding to the position on the chip) inside the aqueous droplets (with a radius $R \sim 80$ μm) for the different concentrations of surfactants used (Fig. 1*E*). The error bars are related to the uncertainty of the calibrations, but each calibration curve shows the same trend (Fig. 1*D*). Because we consider only differences in pH, the errors become less crucial. At low surfactant concentration ($C = 0.05$ mmol/L), the pH remains constant in time. For larger concentrations—here up to 0.69 mmol/L—the pH decreases by more than 1 unit with a typical timescale of the order of 1 s. Qualitatively, this variation of pH corresponds to the transfer of protons from the fluorous phase toward the aqueous phase (*SI Text*). Increasing the surfactant concentration in the fluorous phase has two effects: the pH decreases to a smaller equilibrium value, and the timescale of the process is shorter.

The equilibrium pH is a function of the surfactant concentration: we can conclude that the proton transfer is not limited by the adsorption of the first monolayer to the interface. To determine the surfactant coverage, we measure the critical micellar concentration (CMC). We perform surface-tension measurements using a Wilhelmy plate tensiometer for several surfactant concentrations; the results are displayed in Fig. 2*B*. Indeed, all pH measurements are obtained above the CMC: the equilibrium coverage is constant for all considered concentrations. Therefore, the additional exchange of protons occurs while the interface is at equilibrium coverage, through the desorption of the surfactant and the subsequent adsorption of other surfactant molecules. The surfactant

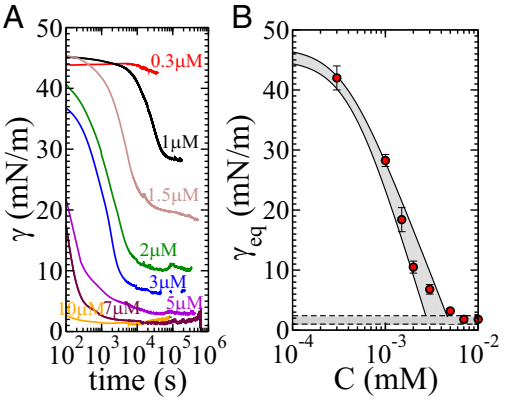

Fig. 2. (*A*) Surface tension data with time for different concentrations. (*B*) Equilibrium surface tension for all concentrations fitting Eq. 6: $\gamma_0 = 46 \pm 1$ mN/m; $\Gamma_\infty = 8.0 \pm 1.0$ μmol/m^2; $\kappa = 7 \pm 1 \times 10^6$ m^6/mol^2; CMC = 4 ± 1 μM; $\Gamma_{eq}^{CMC} = 7.9$ μmol/m^2.

desorption involves the extraction of a counter ion from the aqueous phase to guarantee electroneutrality. Considering the typical ion concentrations in the droplets, the extraction of the Na^+ ions is the most likely event. The overall process can therefore be modeled as

$$\mathrm{KryCOOH_{fl}} \rightleftharpoons \mathrm{KryCOO^-_{int}} + \mathrm{H^+_{aq}}$$
$$\mathrm{Na^+_{aq}} + \mathrm{KryCOO^-_{int}} \rightleftharpoons \mathrm{KryCOONa_{fl}},$$

where *fl* refers to the oil phase, *aq* to the aqueous phase, and *int* to the interface. This model relies on the assumption that the dissociation of the carboxylic acid and the diffusion of the protons (31) inside the aqueous phase are instantaneous compared with the adsorption of the surfactant.

Failure of the Langmuir Adsorption Model. We now quantitatively analyze the reaction rate, the equilibrium of the reaction and the order of the reaction. The initial reaction rate is not a linear relationship with surfactant concentration (Fig. 1*F*). For a Langmuir process of adsorption on a droplet of radius R, we relate the rate of adsorption to the rate of pH change through the surfactant mass conservation at the interface, leading to (*SI Text*):

$$\frac{V}{S}\frac{d[H^+]}{dt} = k_{ads}\left(C_0 - \frac{1}{q}[H^+]\right)\times(\Gamma_\infty - \Gamma), \qquad [1]$$

where V and S are the volume and surface area of the droplet, respectively, C_0 is the initial concentration of the surfactant, and q is the volumetric ratio between the fluorous and the aqueous phase that accounts for dilution effects: were all H^+ transferred from the oil to the water, the concentration in the water would simply be qC_0. When the timescales for surface adsorption and pH change are well-separated, the relaxation of the pH in the droplet is exponential and the initial velocity $d[H^+]/dt|_{t=0}$ in the droplet is expected to be linear in surfactant concentration (Eq. **1** and *SI Text*). Experimentally, we find a square dependence of the initial rate, indicating that the adsorption process does not follow a simple Langmuir process (Fig. 1*F*). The dependence of the initial reaction rate with the concentration requires the modeling of adsorption with a second-order reaction. At this stage, the microscopic details leading to this isotherm remain elusive.

Construction of the Second-Order Adsorption Model. We construct a consistent model for the adsorption process and for the pH variation based on our experimental results. We propose a rate equation where the rate of proton transfer is proportional to the square of the surfactant concentration:

$$\frac{1}{2}\frac{V}{S}\frac{d[H^+]}{dt} = k_{ads}\left(C_0 - \frac{1}{q}[H^+]\right)^2\times(\Gamma_\infty - \Gamma). \qquad [2]$$

For consistency in the model, and because there is no physical reason to assume that the H^+ transfer is independent of the adsorption of surfactant, the straightforward model for adsorption with the adsorption and desorption constant, k_{ads} and k_{des}, respectively, is

$$\frac{1}{2}\frac{d\Gamma}{dt} = k_{ads}C_0^2\times(\Gamma_\infty - \Gamma) - k_{des}\Gamma. \qquad [3]$$

Using the assumption that we have a separation of timescales between the adsorption process and the pH change in the droplet, the interface is quickly reaching equilibrium (denoted as *eq*), whereas the pH is changing slowly. Therefore, as previously, the pH change occurs for $\Gamma = \Gamma_{eq}$. Eq. **2** is therefore a second-order kinetic law leading to the H^+ variation as

$$\frac{\Delta[H^+]}{\Delta[H^+]_{eq}} = \frac{t/\tau_{pH}}{1 + t/\tau_{pH}}$$
$$\text{with}\quad \tau_{pH} = \frac{qR}{6k_{ads}C_0(\Gamma_\infty - \Gamma_{eq})}. \qquad [4]$$

To quantitatively check the validity of our model, we have fitted all experimental data with Eq. **4** using $\Delta[H^+]_{eq}$ and τ_{pH} as fitting parameters (Fig. 3 *A–H*). First, we find that the equilibrium value $\Delta[H^+]_{eq}$ scales linearly with the concentration of surfactant (Fig. 3*I*). This result implies the full transfer of protons from the oil to the droplet, while the interface is at equilibrium. Second, we find that the timescale τ of the process scales as $1/C_0$, as expected for a second-order process (Fig. 3*J*). Combining these results, we recover that the initial speed of the reaction scales as C_0^2. In principle, for a full transfer of protons from the oil to the droplet, we expect $\Delta[H^+]_{eq} = qC_0$, where q is the ratio of the oil-to-water volume fractions. Experimentally, we find that this ratio is ~8, whereas we impose a ratio of flow rates of 5. The error might come from the difficulty to determine accurately the concentration of the carboxylic acid polymer (*SI Text*). However, the experimental data are in good quantitative agreement with our model.

Bulk Equilibrium Data. The measurement of τ_{pH} as a function of C_0 provides a means to determine k_{ads}, provided that both quantities Γ_∞ and Γ_{eq} are known. These two quantities are equilibrium quantities and are measurable using standard characterization techniques (Fig. 2). Using the standard Gibbs isotherm, these measurements provide the values of $\Gamma_{eq}(C), \Gamma_\infty$ and, in addition, the CMC, above which the interfacial coverage stays constant. Based on our model, we fit the experimental data with a second-order model of the form

$$\Gamma_{eq} = \Gamma_\infty\frac{\kappa C^2}{1 + \kappa C^2} \qquad [5]$$

$$\gamma_{eq} = \gamma_0 + \frac{RT\Gamma_\infty}{2}\ln(1 + \kappa C^2). \qquad [6]$$

We here obtain $\Gamma_\infty = 8.0 \pm 1.0$ μmol/m^2, $\kappa = 7 \pm 1 \times 10^6$ m^6 mol^{-2}, and a CMC of $C_{CMC} = 4 \pm 1$ mmol/m^3. These values lead to the determination of $k_{ads} = (1.4 \pm 1) \times 10^3$ s^{-1} m^6 mol^{-2}. We note that the value of Γ_∞ corresponds to a value obtained for small head groups, compatible with our molecule and other data from the literature for fluorinated surfactants (32). It should be noted that we used our model for consistency. However, a standard Langmuir isotherm would provide the same value for Γ_∞ and also shows that—contrary to our microfluidic method—equilibrium measurements do not provide a means to discriminate possible isotherm models. Our experiments provide a measurement of the adsorption constants, provided that the equilibrium is independently determined through standard measurements. The same isotherm model is used to describe the equilibrium and the kinetics of pH change in the droplet, which enables the straightforward use of the equilibrium constants in the microfluidic experiments in a consistent manner.

Impact on Coalescence. In the previous sections, we have measured the adsorption rate using pH measurement on timescales of a several seconds. One of the conclusions is that the timescale of the adsorption of the first monolayer of surfactant is fast, of the order of 10 ms. In the following, we compare this timescale and the timescale required to stabilize an emulsion against coalescence. These measurements of coalescence are obtained

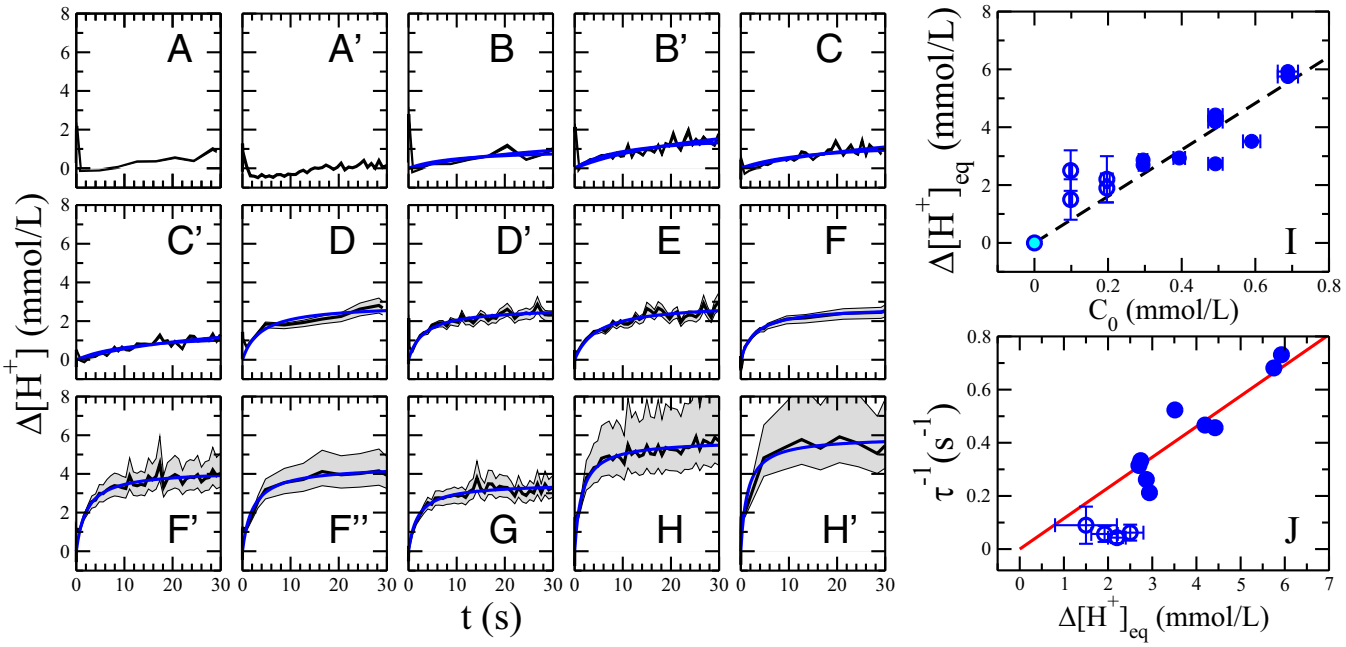

Fig. 3. (*A*–*H*) Change of proton concentration inside the aqueous droplet with time using different concentrations of surfactant (carboxylic acid; Krytox) in the fluorous phase: 0.05 mM (*A*), 0.10 mM (*B*), 0.20 mM (*C*), 0.29 mM (*D*), 0.39 mM (*E*), 0.49 mM (*F*), 0.59 mM (*G*), and 0.69 mM (*H*), with ′ and ″ representing repetitions of the same experimental condition. The black lines show the data calculated from the mean calibration curve with the gray shaded areas relating to the maximum and minimum calibration curves (Fig. 1*D*). (*I*) Fitted equilibrium change of proton concentrations ($\Delta[H^+]_{eq}$; fitted values) for all concentrations of surfactant used. The light blue symbol is set to zero because no pH change takes place when no acidic surfactant is present. (*J*) Fitted τ^{-1} for all concentrations of surfactant. (*I* and *J*) The fitting of the data of the small concentrations (*B* and *C*) is less confident because the pH change is very small. Thus, the fitting value of $\Delta[H^+]_{eq}$ is varied manually to obtain a range of fits.

during the very early kinetics ($t < 200$ ms), which is consistent with the timescale of the adsorption of the first monolayer. The quantitative results are discussed in the following. For these experiments, we use the same fluorous and aqueous phases as above, to determine the transition between stable and unstable emulsions in flow, based on our previous analysis (29). Several chips were produced in which droplets flow without contact in a channel of length L. In these chips, we vary the surfactant concentration and the droplet speed U to change the incubation time of the droplets ($t = L/U$) with a radius $R \sim 35$ μm. The critical parameter that controls the separation between stable and unstable emulsions is the parameter LC^2 (29). Here, this parameter is proportional to the speed of the droplet U (Fig. 4). Therefore, the coalescence experiments lead to the definition of a timescale for the stabilization of the interface of the form: $\tau = 1/(kC^2)$, where $k \sim 909$ s^{-1} m^6 mol^{-2}. We can reuse the rate equation for Γ (Eq. **3**) to compare the stabilization time of the interface during microfluidic emulsification to the adsorption process. Rewriting Eq. **3**, the parameter LC_0^2/U is expressed above the CMC as a function of the adsorption rate constant k_{ads}, the equilibrium interfacial coverage at the CMC Γ_{eq}^{CMC} and Γ_∞ (Fig. 2 and *SI Text*):

$$\frac{L}{U}C_0^2 \approx -\frac{1}{2 \cdot k_{ads}} \ln\left(1 - \frac{\Gamma}{\Gamma_{eq}^{CMC}}\right). \qquad [7]$$

We can now determine Γ from the parameter LC^2/U. Fig. 4*G* shows the lines of iso-Γ superimposed to the coalescence data: the stabilization of the emulsion occurs when the coverage of the interface is close to its equilibrium coverage (in the range of 90–95%).

Discussion

The values extracted from the pH measurement on-chip provide a quantitative description of the kinetics of stabilization and of transfer across the interface in a unified picture. The value of k_{ads} is obtained from the pH measurements for a process occurring at a timescale of several seconds. The value is, however, directly usable to predict the short-time kinetics of surfactant adsorption in coalescence experiments, where the timescale is now one to two orders of magnitude smaller (of order tens of milliseconds). This comparison implied that the coverage stabilizing emulsions in microchannels is close to the equilibrium coverage. Because all of our experiments were performed above the CMC of the surfactant, these results are consistent with the experimental observations that emulsions in microfluidics are hardly stabilized with surfactant concentrations below the CMC (i.e., for equilibrium coverages much smaller than 90%). The experiments show that the adsorption of the first monolayer of surfactant as well as the change of pH are limited by the second-order adsorption kinetics. Thus, the mass transport occurs at a smaller timescale. The timescale for the transport of the surfactant to a clean interface is of the order of tens of milliseconds using an *Sh* of 47–87 (*SI Text*) (28). The calculated timescales of mass transfer and adsorption are of the same order of magnitude. These theoretical timescales give only a rough estimate as a result of uncertainties in the diffusion coefficient as well as the adsorption coefficient. The experiments however are fully consistent with a kinetic-limited model. The practical consequence for emulsification in microfluidics is that although channels can be designed to give enough time for the surfactant to adsorb at the interface, the chemical binding to the interface is the key parameter determining the emulsion stabilization timescale.

An important consequence of our analysis is that we also model the kinetics of equilibration of the chemical potential across the interface (33–35). The transfer of protons toward the aqueous droplet is balanced by the extraction of a counter ion from the droplet to the oil. We have shown recently that no barrier to partitioning could be measured at the timescale of about 45 s (17): the timescale for the establishment of the chemical equilibrium across the interface is therefore smaller. Here we show that the

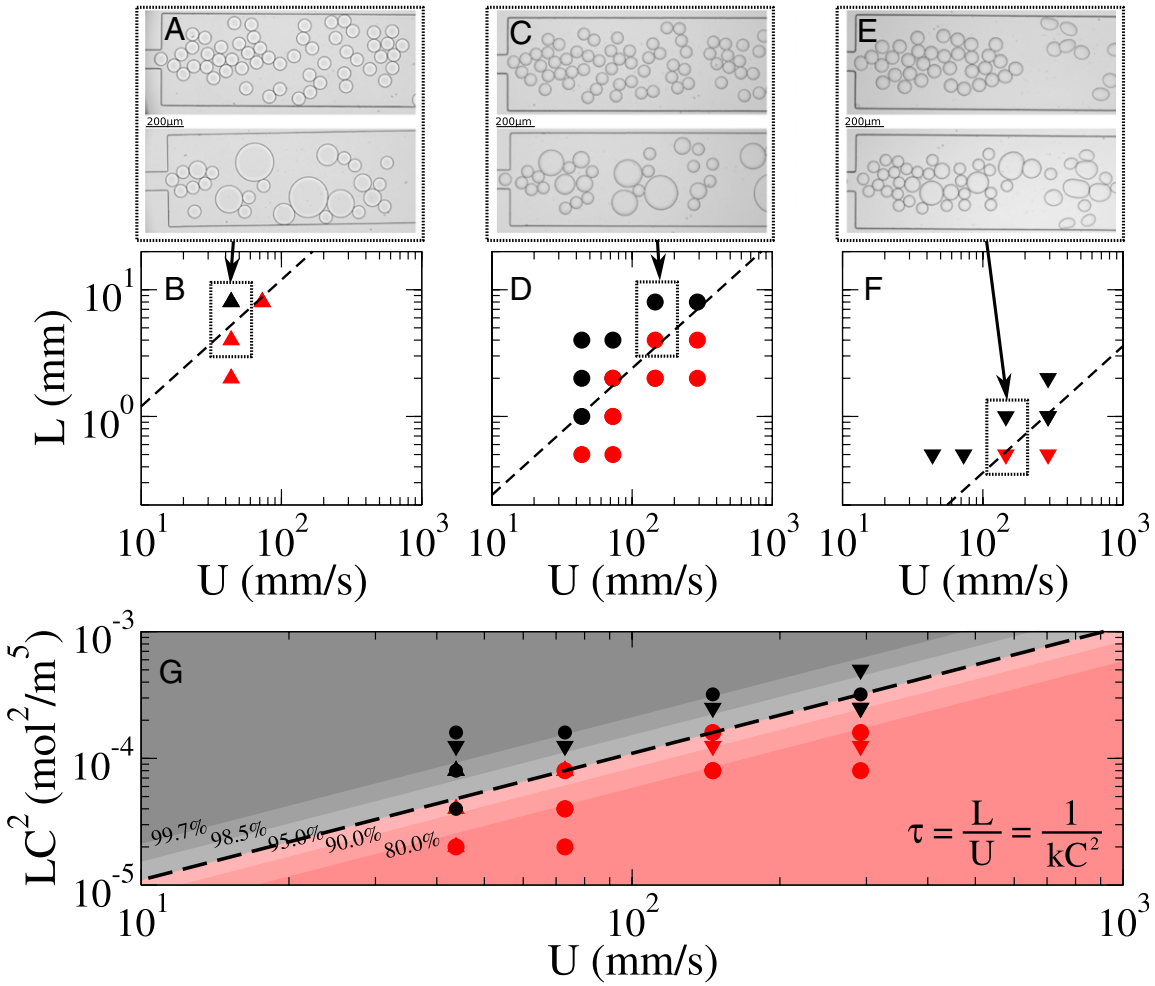

Fig. 4. Coalescence experiments at different distances from the production of droplets L and different speeds U. Stable (black) and unstable (red) droplets are produced at different concentration C of the surfactant [0.10 mM (*B*), 0.20 mM (*D*), and 0.49 mM (*F*); the droplets are stable if less than 1.5% of the droplets coalesce]. The corresponding images are shown in *A*, *C*, and *E*. Depending on the concentration of surfactant, the transition from stable to unstable interfaces takes place at different times t [dashed lines: $t = L/U = 0.12$ s (*B*), $t = 0.024$ s (*D*), and $t = 0.0036$ s (*F*)]. (*G*) The data from *B*, *D*, and *F* scale linear with $LC^2 = 0.0011$ s mol^2/m^{-6} $\times$ U (dashed line). The different symbols refer to the different concentrations (related to the symbols in *B*, *D*, and *F*). The coverage Γ/Γ_{eq}^{CMC} of the interface for different values between 80.0% and 99.7% is represented by the lines of iso-Γ (Eq. **7**).

equilibrium is reached in a couple of seconds at most (~5 s; Fig. 1), for a process involving the full transfer of the ions from one phase to the other. We can now quantify the rate of extraction of ions. According to Eq. **3**, if we consider the transport of the counter ion Na^+ from the droplet toward the oil at steady state, the timescale of the process will simply be the same as the pH-variation timescale. Therefore, we can expect equilibration of positively charged ions to occur as fast as a couple of seconds. This timescale could be considered as a limit for small organic molecule, as observed in previous experiments (17), and this effect has to be taken into consideration when optimizing surfactant formulations. Finally, our method is currently limited to the analysis of carboxylic acid surfactants. However, the transport of organic molecules by surfactant molecules could in principle be used to generalize the method to obtain a universal method of adsorption/desorption constants using an appropriate choice of the pair surfactant/fluorescent dye.

Conclusion

We have designed a microfluidic method to measure the dynamics of adsorption of surfactants to the droplet interface based on droplet pH. With this method, the adsorption kinetics is measured directly, because the transport in the bulk is fast due to the small size of the droplet and the convection associated with the droplet motion in a microchannel. The adsorption process—modeled as a second-order Langmuir process—determines the timescale of the bulk equilibration of the pH. With our results, we make a quantitative link between the process of adsorption/desorption and the kinetics of partitioning, which are two problems of relevance in emulsification. These processes can indeed be described within the same framework. In brief, for our surfactant, for all processes occurring at timescales larger than 1 s, we can safely assume that phase partitioning across the interface is established at all times. In contrast, for processes shorter than 1 s, the dynamics of the chemical equilibration has to be considered. In the general case, the timescale of chemical equilibration is controlled by the ratio of a typical dimension, the radius of the droplet R, and a typical speed $k_{ads}C(\Gamma_\infty - \Gamma_{eq})$. In our experiments, the timescale is at least one to two orders of magnitude larger than the kinetics of equilibration of the surfactant layer itself, of order $(k_{ads}C^2 + k_{des})^{-1}$. This latter timescale corresponds to the time required to cover 90% of the interface, thereby preventing droplet coalescence.

Materials and Methods

Microfluidic Device Fabrication. We manufacture microfluidic devices in poly(methyl methacrylate) (PMMA) and polydimethylsiloxane (PDMS) (*SI Text* and Figs. S4 and S5). The PMMA microfluidic devices are used for the pH

measurements. The PDMS device for the coalescence experiments (Fig. S5) is produced using standard photo- and soft-lithography (36, 37).

Device Operation. Liquids are injected into the channels through glass syringes (Hamilton) connected to the chips via tubings. The syringes are actuated by syringe pumps (Nemesys; Cetoni) at constant speed. For the pH-change experiments, the flow rates are fixed to 7.5 μL/min and 1.5 μL/min for the oil phase and aqueous phase, respectively. For the coalescence experiments, the total flow rates are varied from 10.5 μL/min to 70 μL/min with a flow rate ratio of $q = q_{fl}/q_{aq} = 6$, where q_{fl} and q_{aq} are the flow rates of the fluorous and aqueous phase, respectively. In all cases, the droplets are produced in the dripping regime. The experiments are performed at room temperature (23 ± 1 °C).

Emulsification System. We produce water-in-oil emulsions using an aqueous dispersed phase and a fluorous continuous phase. The aqueous phase consists of a buffer solution (9.5 mM PBS, 0.146 M sodium chloride, pH ∼ 7.3; Sigma-Aldrich) with the pH-sensitive dye SNARF-1 (30) (Life Technologies) at 10 μM. The continuous phase contains the fluorous solvent [3-ethoxyperfluoro (2-methylhexane); Novec7500; 3M] and the acidic surfactant (PFPE with a carboxylic head group; KrytoxFSL; DuPont) with varying concentrations of 0.01 mM, 0.02 mM, 0.03 mM, 0.05 mM, 0.10 mM, 0.20 mM, 0.29 mM, 0.39 mM, 0.49 mM, 0.59 mM, 0.69 mM, and 2.0 mM. The mean molar mass of KrytoxFSL is 1,646 g/mol ± 67 g/mol, as determined using electrospray ionization MS (ESI-MS) and [^{1}H] NMR spectroscopy (Fig. S6).

On-Chip Fluorescence Measurement and Data Processing. We use a laser-induced fluorescence setup as adapted from Baret et al. (38) to determine the pH inside the droplets. Details on the optical system are provided in Fig. S2.

pH Calibration. We use solutions of PBS with known pH values of 5.46, 5.70, 5.84, 6.04, 6.31, 6.72, 7.10, 7.31, 7.66, 7.94, and 8.05. The titration curve of the PBS solution is measured using a standard pH meter (Orion, Star121; Thermo Scientific) (*SI Text* and Fig. S7). The variations in the calibrations are averaged over two runs, which determines the error bar in the calibration. The calibration is performed where the droplets have reached this terminal velocity (9.8 mm ≙ 0.5 s after production) (39). We use the same flow rates for all experiments to avoid bias (39).

On-Chip Time-Dependent pH Measurements. The kinetics of the pH change in droplet is measured by recording the ratio of droplet fluorescence I_{647}/I_{580} at positions along the channel corresponding to different times given by the channels cross-section and the total flow rates.

Equilibrium Surface-Tension Measurement. Time-dependent surface tensions are measured at the oil–water interface using a Wilhelmy plate configuration (Wilhelmy plate platinum; wetted length, 39.24 mm; KSV-Nima LL, KN-ISR-2 Langmuir Trough; LOT-QuantumDesign). For all concentrations, the experiments are equilibrated over several hours at 25 °C. For the smallest concentration ($C = 0.3$ μM), no equilibrium could be reached over 11 days.

ACKNOWLEDGMENTS. Fruitful discussions with Dr. M. Brinkmann and Prof. S. Koester are warmly acknowledged. We also thank Uwe Plessmann for help with the ESI-MS measurements and W. Keiderling and A. Gerke at the Workshop Facility of the Max Planck Institute for Dynamics and Self-Organization for technical support. J.-C.B. acknowledges support from European Research Council (ERC) Seventh Framework Programme (2007–2013) ERC Grant Agreement 306385–SOFt Interfaces; from the "Région Aquitaine"; and from the French Government "Investments for the Future" Programme, University of Bordeaux Initiative of Excellence (IDEX Bordeaux) [Reference Agence Nationale de la Recherche (ANR)-10-IDEX-03-02]. B.R. also acknowledges fellowship funding from the International Max Planck Research Schools for Physics of Biology and Complex Systems. B.R. and P.G. acknowledge additional support from the Georg-August-Universität Göttingen doctoral school.

1. Franklin B (1774) Of the stilling of waves by means of oil (extracted from sundry letters). *Phil Trans* 64:445–460.
2. Rosen MJ (2004) *Surfactants and Interfacial Phenomena* (John Wiley & Sons, Hoboken, NJ).
3. Bibette J, Leal-Calderon F, Poulin P (1999) Emulsions: Basic principles. *Rep Prog Phys* 62:969–1033.
4. Bremond N, Bibette J (2012) Exploring emulsion science with microfluidics. *Soft Matter* 8:10549–10559.
5. Theberge AB, et al. (2010) Microdroplets in microfluidics: An evolving platform for discoveries in chemistry and biology. *Angew Chem Int Ed Engl* 49(34):5846–5868.
6. Baret JC (2012) Surfactants in droplet-based microfluidics. *Lab Chip* 12(3):422–433.
7. Kelly BT, Baret JC, Taly V, Griffiths AD (2007) Miniaturizing chemistry and biology in microdroplets. *Chem Commun (Camb)* 38(18):1773–1788.
8. Agresti JJ, et al. (2010) Ultrahigh-throughput screening in drop-based microfluidics for directed evolution. *Proc Natl Acad Sci USA* 107(9):4004–4009.
9. Pekin D, et al. (2011) Quantitative and sensitive detection of rare mutations using droplet-based microfluidics. *Lab Chip* 11(13):2156–2166.
10. Joensson HN, Andersson Svahn H (2012) Droplet microfluidics–A tool for single-cell analysis. *Angew Chem Int Ed Engl* 51(49):12176–12192.
11. Guo MT, Rotem A, Heyman JA, Weitz DA (2012) Droplet microfluidics for high-throughput biological assays. *Lab Chip* 12(12):2146–2155.
12. Miller R, Kretzschmar G (1991) Adsorption kinetics of surfactants at fluid interfaces. *Adv Colloid Interface Sci* 37:97–121.
13. Dai B, Leal L (2008) The mechanism of surfactant effects on drop coalescence. *Phys Fluids* 20:040802.
14. Taylor P (1995) Ostwald ripening in emulsions. *Colloids Surf A Physicochem Eng Asp* 99:175–185.
15. Skhiri Y, et al. (2012) Dynamics of molecular transport by surfactants in emulsions. *Soft Matter* 8:10618–10627.
16. Gruner P, et al. (2015) Stabilisers for water-in-fluorinated-oil dispersions: Key properties for microfluidic applications. *Curr Opin Colloid Interface Sci* 20:183–191.
17. Gruner P, et al. (2016) Controlling molecular transport in minimal emulsions. *Nat Commun* 7:10392.
18. Ward A, Tordai L (1946) Time dependence of boundary tensions of solutions I. The role of diffusion in time effects. *J Chem Phys* 14:453–461.
19. Langmuir I (1917) The shapes of group molecules forming the surfaces of liquids. *Proc Natl Acad Sci USA* 3(4):251–257.
20. Diamant H, Andelman D (1996) Kinetics of surfactant adsorption at fluid-fluid interfaces. *J Phys Chem* 100:13732–13742.
21. Borwankar RP, Wasan DT (1988) Equilibrium and dynamics of adsorption of surfactants at fluid-fluid interfaces. *Chem Eng Sci* 43:1323–1337.
22. Kalinin VV, Radke CJ (1996) An ion-binding model for ionic surfactant adsorption at aqueous-fluid interfaces. *Colloids Surf A Physicochem Eng Asp* 114:337–350.
23. Kretzschmar G, Miller R (1991) Dynamic properties of adsorption layers of amphiphilic substances at fluid interfaces. *Adv Colloid Interface Sci* 36:65–124.
24. Moorkanikkara SN, Blankschtein D (2009) New methodology to determine equilibrium surfactant adsorption properties from experimental dynamic surface tension data. *Langmuir* 25(11):6191–6202.
25. Alvarez NJ, Vogus DR, Walker LM, Anna SL (2012) Using bulk convection in a microtensiometer to approach kinetic-limited surfactant dynamics at fluid-fluid interfaces. *J Colloid Interface Sci* 372(1):183–191.
26. Eastoe J, Dalton JS (2000) Dynamic surface tension and adsorption mechanisms of surfactants at the air-water interface. *Adv Colloid Interface Sci* 85(2-3):103–144.
27. Jin F, Balasubramaniam R, Stebe K (2004) Surfactant adsorption to spherical particles: The intrinsic length scale governing the shift from diffusion to kinetic-controlled mass transfer. *J Adhes* 80:773–796.
28. Mikaelian D, Haut B, Scheid B (2015) Bubbly flow and gas-liquid mass transfer in square and circular microchannels for stress-free and rigid interfaces: Dissolution model. *Microfluid Nanofluidics* 19:899–911.
29. Baret JC, Kleinschmidt F, El Harrak A, Griffiths AD (2009) Kinetic aspects of emulsion stabilization by surfactants: A microfluidic analysis. *Langmuir* 25(11):6088–6093.
30. Han J, Burgess K (2010) Fluorescent indicators for intracellular pH. *Chem Rev* 110(5): 2709–2728.
31. Agmon N (1995) The Grotthuss mechanism. *Chem Phys Lett* 244:456–462.
32. Brosseau Q, Vrignon J, Baret JC (2014) Microfluidic dynamic interfacial tensiometry (mudit). *Soft Matter* 10(17):3066–3076.
33. Chen Y, Wijaya Gani A, Tang SK (2012) Characterization of sensitivity and specificity in leaky droplet-based assays. *Lab Chip* 12(23):5093–5103.
34. Janiesch JW, et al. (2015) Key factors for stable retention of fluorophores and labeled biomolecules in droplet-based microfluidics. *Anal Chem* 87(4):2063–2067.
35. Sandoz PA, Chung AJ, Weaver WM, Di Carlo D (2014) Sugar additives improve signal fidelity for implementing two-phase resorufin-based enzyme immunoassays. *Langmuir* 30(23):6637–6643.
36. Xia YN, Whitesides GM (1998) Soft lithography. *Annu Rev Mater Sci* 28:153–184.
37. Xia Y, Whitesides GM (1998) Soft Lithography. *Angew Chem Int Ed* 37:550–575.
38. Baret JC, Beck Y, Billas-Massobrio I, Moras D, Griffiths AD (2010) Quantitative cell-based reporter gene assays using droplet-based microfluidics. *Chem Biol* 17(5):528–536.
39. Vazquez B, Qureshi N, Oropeza-Ramos L, Olguin LF (2014) Effect of velocity on microdroplet fluorescence quantified by laser-induced fluorescence. *Lab Chip* 14(18):3550–3555.
40. Dick JG (1973) *Analytical Chemistry, International Student Edition* (McGraw-Hill Kogakusha, Tokyo).
41. Bliefert C, Linek A, Morawietz G (1978) *pH-Wert-Berechnungen* (Verlag Chemie GmbH, Weinheim, Germany).
42. Press W, Teukolsky S, Vetterling W, Flannery B (2007) *Numerical Recipes: The Art of Scientific Computing* (Cambridge Univ Press, Cambridge, UK), 3rd Ed.
43. Doan V, Köppe R, Kasai PH (1997) Dimerization of carboxylic acids and salts: An IR study in perfluoropolyether media. *J Am Chem Soc* 119:9810–9815.
44. Saboni A, Alexandrova S, Spasic AM, Gourdon C (2007) Effect of the viscosity ratio on mass transfer from a fluid sphere at low to very high Peclet numbers. *Chem Eng Sci* 62:4742–4750.
45. Li JM, Liu C, Liu JS, Xu Z, Wang LD (2009) Multi-layer PMMA microfluidic chips with channel networks for liquid sample operation. *J Mater Process Technol* 209: 5487–5493.